Elastic scattering and breakup of ^{11}Be on protons at 26.9A MeV

J. Chen, J. L. Lou,[*] Y. L. Ye, Z. H. Li, Y. C. Ge, Q. T. Li, J. Li, W. Jiang, Y. L. Sun, and H. L. Zang

School of Physics and State Key Laboratory of Nuclear Physics and Technology, Peking University, Beijing 100871, China

N. Aoi, E. Ideguchi, H. J. Ong, Y. Ayyad, K. Hatanaka, D. T. Tran, T. Yamamoto, M. Tanaka, T. Suzuki, and N. T. Tho

Research Centre for Nuclear Physics, Osaka university, Osaka, Japan

J. Rangel

Instituto de Física, Universidade Federal Fluminense, Av. Litoranea s/n, Gragoatá, Niterói, R.J., 24210-340, Brazil

A. M. Moro

Departamento de FAMN, Universidad de Sevilla, Apartado 1065, E-41080 Sevilla, Spain

D. Y. Pang

School of Physics and Nuclear Energy Engineering, Beihang University, Beijing 100191, China

J. Lee, J. Wu, H. N. Liu, and C. Wen

RIKEN (Institute of Physical and Chemical Research), 2-1 Hirosawa, Wako, Saitama 351-0198, Japan

The elastic scattering and breakup of the halo nucleus ^{11}Be on protons at an incident energy of 26.9A MeV have been measured. The ^{11}Be $+ p$ elastic scattering cross sections at various energies, including the present one, are systematically analyzed with the Chapel Hill 89 (CH89) and Koning-Delaroche (KD) global optical model potentials (OMPs), and the corresponding normalization factors are obtained. An extended version of the continuum-discretized coupled-channels (XCDCC) formalism, including dynamic core excitation effects, is applied to analyze the elastic scattering and breakup data. It is found that the core excitation plays a moderate role in the elastic scattering and breakup reaction of the halo nucleus ^{11}Be, being consistent with previous results at higher energies.

I. INTRODUCTION

With the availability of radioactive beams for the nuclei far from stability, the investigation of neutron-rich nuclei close to the drip line has become a subject of great interest, owing to the novel properties of these nuclei as compared to those for ordinary nuclei [1–4]. Among these exotic systems, neutron-halo nuclei have received special attention. These are very weakly bound systems, consisting of a tightly bound core surrounded by one or two weakly bound neutrons, giving rise to a dilute, spatially extended system [5–7]. For example, the halo nucleus ^{11}Be is usually interpreted as a ^{10}Be core surrounded by a loosely bound valence neutron. Because of its low binding energy ($S_n = 0.504 \pm 0.006$ MeV), the valence neutron in ^{11}Be orbits at a relatively large distance from the core (~ 5.7 fm in average according to Ref. [8]). Furthermore, the $1/2^+$ ground state (g.s.) and the $1/2^-$ first excited state in ^{11}Be are inverted with respect to the level scheme predicted by the conventional independent particle model. It is also known that the ground state may have a configuration of $[^{10}\text{Be(g.s.)} \otimes 1s_{1/2})]$, with a probability of about 60%–80%, according to several knockout [9], transfer [10], and Coulomb dissociation [11] experiments. These experiments [9,11], as

well as different theoretical models [12], indicate the existence of a sizable $[^{10}\text{Be}(2^+) \otimes 1d_{5/2}]$ configuration, in which the core is excited.

It was realized that, not only the nuclear structure, but also the reaction dynamics can be largely affected by the weak binding of the halo nuclei. For instance, the coupling to the breakup channel is usually strong and should be accounted for by the reaction formalism, such as the continuum-discretized coupled-channels (CDCC) method [13,14]. In addition to the influence of the continuum states, it was recently found that the core excitation in halo nuclei may also cause significant changes in nuclear structure as well as in nuclear reaction dynamics [15]. The core excitation mechanism was implemented in an extended version of the CDCC formalism (XCDCC) proposed by Summers *et al.* [15] and in a no-recoil extended DWBA model (XDWBA) [16]. It is worth noting that the CDCC and XCDCC methods provide only the description of the so-called elastic breakup, in which the dissociated fragments from the projectile all emit out while the target remains in the ground state. A calculation using the XDWBA method has demonstrated the significant effect of the core excitation in the case of the breakup of ^{11}Be on a proton target at an incident energy of 63.7A MeV [16,17]. This result was later confirmed by a XCDCC calculation [18]. The ^{11}Be $+ p$ reaction was also measured at 49.3 [19] and 38.4A MeV [20], but only the elastic scattering data were reported. So far the experimental evidence

---

[*]jllou@pku.edu.cn

showing the importance of the core excitation in the reaction processes is very limited and it would be of timely importance to confirm whether this effect persists for other systems and energies. We provide here new experimental results at a lower energy, together with the corresponding theoretical analysis.

In Secs. II and III of this article, we present the results from a new experiment of elastic scattering and breakup of ^{11}Be on a proton target at $26.9A$ MeV. First, to obtain a reliable optical model potential (OMP) of ^{11}Be $+ p$, we systematically analyzed the ^{11}Be $+ p$ elastic scattering data at four energies, namely 26.9, 38.4, 49.3, and $63.7A$ MeV [21], and the obtained normalization factors of the CH89 [22] and KD [23] global OMPs are reported in Sec. IV. In Sec. V, we present the theoretical analysis using the XCDCC formalism to investigate the effects of dynamic core excitation on the elastic scattering and breakup reaction at this incident energy. The summary will be given in Sec. VI.

II. EXPERIMENTAL SETUP

The experiment was performed at the EN-course beam line at RCNP (Research Center for Nuclear Physics), Osaka University [24]. The ^{11}Be beam at $26.9A$ MeV was produced from a primary beam of ^{13}C at $60A$ MeV impinging on a 456-mg/cm^2 Be target and purified by the electromagnetic separator with a 650-mg/cm^2 aluminium degrader. The secondary beam intensity was approximately 10^4 particles per second (pps) with a purity of about 95% for ^{11}Be, and a contamination of about 5% for ^{9}Li. The momentum spread was limited, by a slit, down to $\Delta P/P \leqslant 1\%$ to reduce the energy uncertainty of the beam.

The ^{11}Be beam was scattered from a 4-mg/cm^2 polypropylene target $(CH_2)_n$ and a 4-mg/cm^2 deuterated polypropylene $(CD_2)_n$, both tilted for $15°$ to restrict the energy loss of the detected light particles in the target. To subtract the background arising from the ^{12}C in the $(CH_2)_n$ and $(CD_2)_n$ target, some separate measurements were performed with a ^{12}C target. Two parallel plate avalanche counters (PPACs) upstream of the target provided tracking information for the incoming beam, with an overall efficiency of about 90%. The position resolution of the PPACs was about 1.5 mm (FWHM), and the distance between them was about 672 mm, resulting in an angular deviation less than $0.3°$. A plastic scintillator, providing the energy loss (ΔE) and time-of-flight (TOF) information, from which ^{11}Be is well separated from the contamination in the beam, was installed at about 1.0 m upstream from the reaction target.

The setup of detectors of this experiment is schematically shown in Fig. 1. There are three charged particle telescopes (TELE0, TELE1, TELE2) and a set of annular silicon detectors (ADSSD). TELE0, TELE1, and TELE2 were used to detect the Be isotopes around $0°$, the recoiled protons and deuterons, and the reaction-produced charged fragments at forward angles, respectively. ADSSD was installed at backward angles to detect the protons from the ^{11}Be$(d,p)^{12}$Be transfer reaction.

TELE0, comprising a double-sided silicon strip (DSSD) detector with a thickness of 1000 μm and two large surface silicon detectors (SSD) of 1500-μm thick, was centered at the beam spot. TELE1 was placed around $76°$ with
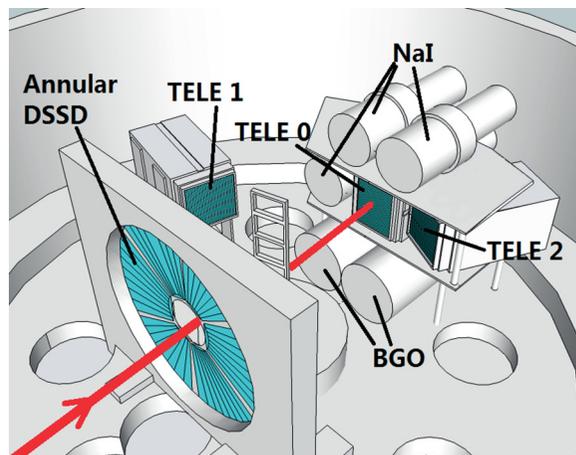

FIG. 1. Schematic view of the experimental setup. The red arrow indicates the direction of the incoming beam, and the blue areas exhibit the active areas of the silicon detectors.

respect to the beam direction, which was composed of a 300-μm DSSD, a 1500-μm SSD, and a layer of four CsI(Tl) crystals read out by photodiodes. Each DSSD is divided into 32 strips on both sides and has an active area of 62.5×62.5 mm^2. The distances between the center of the target and those of the telescopes are 200 and 170 mm for TELE0 and TELE1, respectively. As a result, the angular resolution in the experiment is approximately $0.8°$ (FWHM), taking into account the angular resolution resulting from the PPACs. The energy resolution for the silicon detectors was less than 1% for α particles at 5.486 MeV, which is good enough to discriminate the isotopes lighter than carbon, with the standard $\Delta E - E$ method. A 1.0-MeV threshold was set for the scattered protons and deuterons to cut down the noise. In addition, ADSSD was positioned 135 mm from the reaction targets. TELE2, having the same composition as TELE1, was placed around $25°$ with a distance of 235 mm from the target.

In this paper, we will focus on the elastic scattering and breakup of ^{11}Be on protons, which are basically related to the detection by TELE1 and TELE0 accordingly.

III. EXPERIMENTAL RESULTS

The experiment was performed in inverse kinematics, in which the projectilelike fragments emitted at forward angles were measured in coincidence with the recoiled protons or deuterons to have a better discrimination of various reaction channels. The particle identification(PID) performance from TELE0 is shown in Fig. 2. The location for ^{10}Be was checked with the simulation and the PID from other reaction channels, such as elastic scattering of ^{11}Be $+d$, in which the ^{10}Be isotope loci is well separated from the nearby ^{11}Be. Recoiled protons in coincidence with the forward moving ^{11}Be or ^{10}Be (see Fig. 2) correspond to the scattering to the bound states (g.s. and 320-keV excited state) or the inelastic scattering to the unbound states within $1n$ emission, respectively, of the ^{11}Be nucleus. According to the calculations in Sec. V, the contribution of inelastic scattering to the 320-keV state can be neglected. This means that the cross sections of elastic
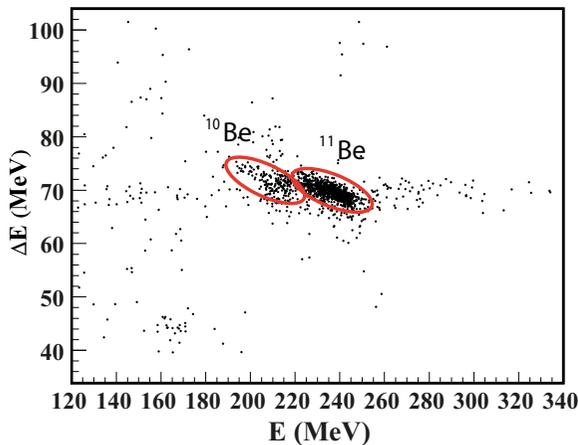
FIG. 2. The PID using data taken by TELE0 in coincidence with protons measured by TELE1.

scattering and breakup can be extracted from recoil protons in coincidence with ^{11}Be and ^{10}Be, respectively.

The kinetic energies and angles of the recoiling protons were measured using TELE1, from which the excitation energy and scattering angles of ^{11}Be in the center-of-mass (c.m.) system were subsequently deduced from two-body kinematics. The protons are assumed to be emitted from the half depth of the target, whose traveling distances and the corresponding energy loss in the target were calculated. In Fig. 3 is plotted the energy versus the scattering angle of protons recoiling into TELE1 in coincidence with ^{11}Be [Fig. 3(a)] and ^{10}Be [Fig. 3(b)], respectively. A cut of laboratory angles smaller than $80°$ was applied because of the detectable energy threshold. Most events lie along the kinematical loci of elastic and inelastic scattering shown by the solid curves.

Note that the CDCC or XCDCC method provides only the elastic breakup cross sections whereas the experimental breakup reaction might contain contributions from other processes, such as striping of one neutron from ^{11}Be [9]. However, with the coincident measurement of the recoil protons in TELE1 and ^{10}Be in TELE0, most of these accompanying reactions could be excluded by using the kinematics condition as illustrated in Fig. 3 and similarly applied in Ref. [25]. For instance, the stripping of one neutron from the ^{11}Be projectile by the proton target would follow approximately the kinematics of the p-n scattering as shown by the dotted curve in Fig. 3(b) [26,27]. For other processes, such as absorption and evaporation, the emitted protons have smaller energies in the c.m. system, and scatter mostly to the forward angles with the Be fragments. Consequently, when applying an excitation energy cut $0.5 < E_{ex} < 3.0$ MeV as described below, our results are almost free from contaminations of stripping and other more complicated processes. Therefore, by using the proton target and with the coincident measurement, our experimental results correspond well to the elastic breakup reaction mechanism provided by the XCDCC approach.

The ^{11}Be excitation energy spectra for the ground state and the continuum states (in the inset) is displayed in Fig. 4, deduced from the scattered protons in coincidence with forward-moving ^{11}Be and ^{10}Be fragment identified by
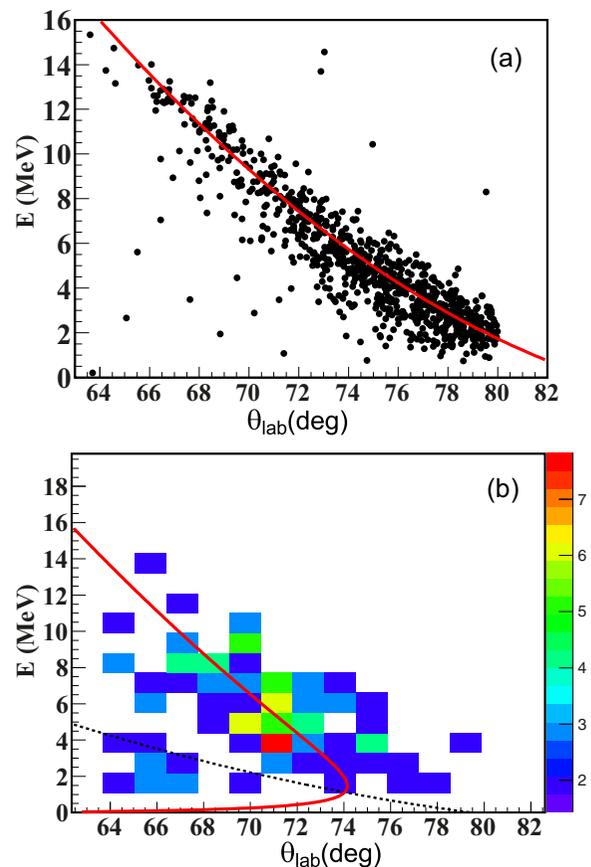

FIG. 3. Bidimensional plot of energy vs angle for recoiling protons in coincidence with ^{11}Be (top) and ^{10}Be (bottom) at forward angles. The kinematic loci for the elastic scattering and inelastic excitation to 1.78-MeV resonance in ^{11}Be are shown as the solid curves in (a) and (b), respectively. The kinematic for protons recoiled from the $n - p$ elastic scattering is also drawn as the dashed line in (b).

TELE0, respectively. The data taken with the carbon target were normalized to the same number of beam particles and equivalent carbon thickness as for the $(CH_2)_n$ target, and used for the background subtraction. The FWHM of the peak for elastic scattering is 1.2 MeV, which agrees with the energy spread obtained from the simulation taking into account the beam, target, and detector effects. As seen in the inset of Fig. 4, the excitation energy spectrum for the breakup channel exhibits a broad peak around 2 MeV, which can partially be attributed to the excitation of the $5/2^+$ resonant state located at 1.78 MeV in ^{11}Be. The excitation energies ranging from -2.0 to 2.0 MeV and from 0.5 to 3.0 MeV were utilized to analyze the differential cross sections of elastic scattering and breakup reaction, respectively. Because of the decreasing angular acceptance of TELE1, we were unable to get meaningful cross sections for excitation energies above 3.0 MeV. Simulations for the geometrical efficiency of the detectors were carried out using the GEANT4 package [28], taking into consideration the beam profile, the target thickness, the energy threshold, dead areas of the silicon strip detectors,
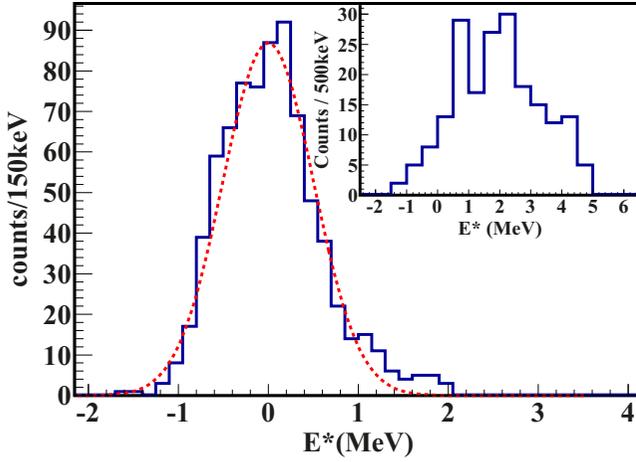
FIG. 4. The excitation energy spectrum for the ground state and the excited states (in the inset) of ^{11}Be integrated over the c.m. angular range of 22° to 45.5°, deduced from the scattered protons in coincidence with ^{11}Be and ^{10}Be in Fig. 2, respectively. The background contributions arising from ^{12}C have been subtracted.

reaction loss in the detector material, and the geometry of TELE0 and TELE1.

The angular distributions of ^{11}Be $+ p$ elastic scattering (as a ratio to the Rutherford cross sections) and breakup cross sections are presented in Figs. 5(a) and 6(b), respectively, with each data point corresponding to an angular width of 1.5° in the laboratory frame. The error bars are purely statistical, including the errors resulting from the background subtraction

of ^{12}C content in the target. The systematic error is less than 10%, considering the uncertainties in geometrical efficiency determination, the thickness of the target, the cut on the PID spectrum as shown in Fig. 2, and the ranges applied on the excitation spectra.

IV. INVESTIGATION OF THE OPTICAL POTENTIAL

Good quality OMPs are not only mandatary for describing the elastic scattering, but also necessary as input for many reaction calculations, such as distorted-wave-Born-approximation (DWBA) and coupled-channel (CC) calculations. Hence it is necessary to investigate the OMP or establish a new systematics when a new scattering channel was experimentally explored. Global OMPs, such as the CH89 and KD potentials, have been extracted from the analysis of proton and neutron elastic scattering data from nuclei with $A \geqslant 40$ and $A \geqslant 24$, respectively. In the case of stable nuclei, these potentials reproduce successfully the experimental data for a wide range of incident energies and target nuclei, even when extrapolated outside their initial domain of validity [19,29]. However, they may be inadequate for reactions with unstable nuclei, which are often carried out in inverse kinematics [19]. The phenomenological OMP for nucleon-nucleus scattering U is usually defined as

$$U(r,E) = V_V(r,E) + iW_V(r,E) + iW_D(r,E)$$
$$+ V_{SO}(r,E).\mathbf{l}.\sigma + iW_{SO}(r,E).\mathbf{l}.\sigma + V_c(r,E), (1)$$

where $V_{V,SO,C}$ and $W_{V,D,SO}$ are the real and imaginary components of the volume-central (V), surface-central (D),
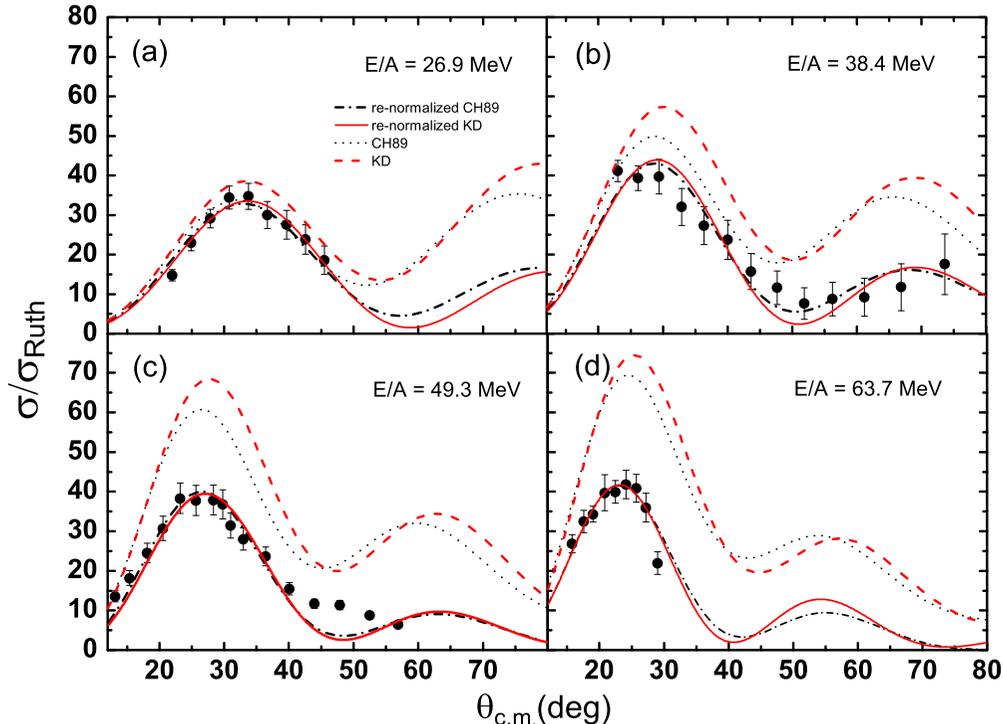

FIG. 5. Differential cross sections of ^{11}Be $+ p$ elastic scattering at four incident energies. The red dashed, black dotted, red solid curves, and black dot-dashed curves display the calculations using KD, CH89, re-normalized KD, and re-normalized CH89 OMPs, respectively.
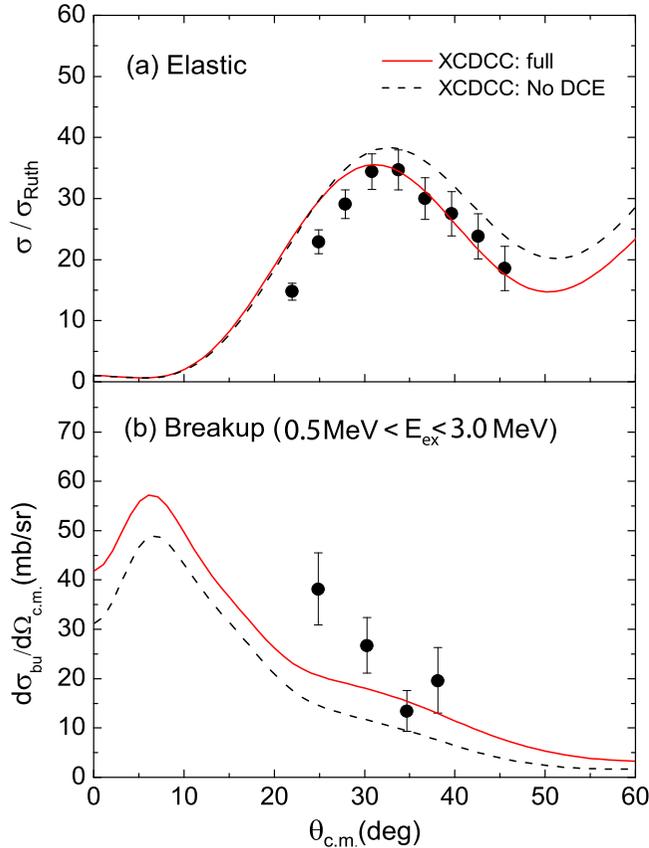
FIG. 6. Experimental and calculated elastic (top) and breakup (bottom) cross sections, as a function of the c.m. scattering angle, for the reaction ^{11}Be+p at 26.9A MeV. The solid lines and the dashed lines are the full XCDCC calculations and the XCDCC calculations without dynamic core excitation (DCE), respectively.

spin-orbit (SO), and Coulomb (C) potentials, respectively. E is the laboratory energy of the incident particle. Normalization factors for the real and imaginary central potentials are often required, case by case, when applied to the scattering of light exotic nuclei such as ^{8}He [30], ^{11}Li [31] or ^{11}Be [19].

Aside from the present data, three sets of ^{11}Be + p elastic scattering data are available in the literature, at energies of 49.3 [19], 38.4 [20], and 63.7A MeV [21]. To improve the agreement with the data, starting from the CH89 and KD global potentials, we applied the normalization factors λ_V and λ_W, respectively, to the real and imaginary parts of the central potentials, i.e., $V_V(r,E)$ and $iW_V(r,E) + iW_D(r,E)$, and the

best normalization-factor values were individually searched at four incident energies using the code SFRESCO [32]. In Fig. 5, are shown the calculated differential cross sections in comparison with the experimental data, while the obtained normalization parameters are listed in Table I. The uncertainty (in the parenthesis) of each factor is obtained from the searching code SFRESCO, corresponding to the standard deviation of the fit. It can be seen that λ_Vs and λ_Ws are consistently smaller and larger than 1, respectively, being consistent with those obtained for other exotic nuclei, such as ^{6,8}He [33] and ^{9,11}Li [19]. This behavior of the normalization factors can be explained by the effect of the coupling to the breakup channels [19,34,35], which is particularly important for loosely bound nuclei. In Fig. 5, we can see the increasing discrepancy between the *non-normalized* calculation and the experimental data, with the increasing incident energy, which might be attributed to the increasing importance of the breakup effects.

V. XCDCC CALCULATIONS

XCDCC is an extended version of the standard CDCC formalism, which takes into account core-excited components in the projectile structure, and also the dynamic core excitation and de-excitation processes during the collision. The model was originally formulated in terms of a binning discretization method for the projectile continuum [15] and, more recently, using a pseudostate (PS) representation [18]. In this work, we employ the latter one.

The ^{11}Be structure is described with the particle-rotor model using the Hamiltonian of Ref. [36] (model Be12-b), which consists of a Woods-Saxon central part, with a fixed geometry ($R_0 = 2.483$ fm, $a = 0.65$ fm) and a parity-dependent strength with $V_c = -54.24$ MeV ($V_c = -49.67$ MeV) for positive (negative) parity states. The potential contains also a spin-orbit term, whose radial dependence is given by the derivative of the central Woods-Saxon part, and strength $V_{so} = 8.5$ MeV. For the ^{10}Be core, this model assumes a permanent quadrupole deformation $\beta_2 = 0.67$ (i.e., $\delta_2 = \beta_2 R_0 = 1.664$ fm). This model reproduces the separation energies of the two-bound states of ^{11}Be as well as the position of the low-lying narrow $5/2^+$ and $3/2^+$ resonances at 1.78 and 3.41 MeV, respectively. Theoretical calculations show that the $3/2^-$ resonance at 2.65 MeV has a negligible effect on the breakup cross sections of ^{11}Be + p [16]. Therefore, the $3/2^-$ resonant state is not taken into consideration in this calculation.

To obtain the energies and wave functions of ^{11}Be we use a PS method. For the relative motion of the valence particle to the core, we use the transformed harmonic oscillator (THO)

TABLE I. Normalization factors applied to the real (V_V) and imaginary ($iW_V + iW_D$) central potentials of KD and CH89 OMPs for ^{11}Be + p elastic scattering at different energies. The uncertainties in these normalization factors are shown in the parentheses, corresponding to the standard deviation of the fit.

Incident energies	λ_V (KD)	λ_W (KD)	χ^2/n (KD)	λ_V (CH89)	λ_W (CH89)	χ^2/n (CH89)
26.9A MeV(present work)	0.73(7)	1.19(12)	0.18	0.78(7)	1.02(9)	0.29
38.4A MeV [20]	0.81(5)	1.32(14)	1.38	0.82(5)	1.07(11)	0.90
49.3A MeV [19]	0.64(2)	1.17(8)	3.80	0.67(2)	1.05(6)	2.80
63.7A MeV [21]	0.70(3)	1.76(22)	0.95	0.70(2)	1.33(16)	0.98

basis, which is obtained applying a local scaled transformation (LST) to the HO basis to transform the Gaussian asymptotic behavior into an exponential form. For the LST, we use the analytical prescription of Ref. [37], which was already applied to ^{11}Be [38], and the parameters used in the present calculations are similar to those employed in that reference. The size of the basis is determined by the number of oscillator functions (N), the maximum orbital angular momentum for the core-valence motion (ℓ), and the number of core states. In the present calculations we use $N = 10, \ell_{max} = 3$, and the first two states of the core (the g.s. and the first excited state). With these parameters, we considered continuum states with total angular momentum $J_p = 1/2^{\pm}$, $3/2^{\pm}$, and $5/2^{+}$. We verified that using a larger value of N, or higher values of J_p, did not change significantly the calculated observations. Furthermore, only eigenvalues with energies below 7 MeV were retained in the coupled-channels calculations because the effect of higher eigenvalues was found to be negligible.

The XCDCC calculations require also the valence-target and core-target interactions. For the former ($p + n$), we used the Tjon IV interaction [39], which contains only central terms, constructed as a superposition of two Yukawa functions. The central part of the core-target interaction, ^{10}Be + p, was generated microscopically by folding the JLM effective interaction with the ^{10}Be ground-state density, obtained from an antisymmetrized molecular dynamics (AMD) calculation [40]. To generate the transition potential between the the ^{10}Be ground state (0^+) and first excited state (2^+) and the $2^+ \rightarrow 2^+$ reorientation coupling, this potential was deformed using a quadrupole deformation length of $\delta_2 = 1.8$ fm, and expanded in multipoles, retaining the monopole and quadrupole terms of the expansion. The JLM folding potential usually requires renormalization factors for the real and imaginary parts. Ideally, these factors could be determined from the analysis of elastic and inelastic data of $p + {}^{10}$Be at the same energy per nucleon of the $p + {}^{11}$Be reaction under study. Because these data are not available, we have determined these factors empirically, by imposing that the calculated $p + {}^{11}$Be elastic differential cross section, obtained with the full XCDCC calculation, reproduces the present elastic data. This yields $N_r \approx 1$ and $N_i \approx 0.64$. These values were adopted for the subsequent calculations.

The calculated differential elastic cross section is compared with the data in Fig. 6 (top). The solid line is the full XCDCC calculation which, with the $p + {}^{10}$Be renormalization factors quoted above, describes reasonably well the data in the full angular range. Compared to the calculation without core excitation, it becomes apparent that the dynamic core excitation effect produces a sizable reduction of the elastic cross section.

The corresponding breakup differential cross sections are plotted in Fig. 6 (bottom). The full XCDCC calculation (full curve) gives the correct trend of the data, but with some underestimation of the magnitude. To illustrate the effect of the dynamic core excitation mechanism (that is, the excitation of the ^{10}Be from its interaction with the proton target), we have performed also a XCDCC calculation keeping only the central part of the ^{10}Be + p interaction. Note that, in this calculation, the ^{10}Be deformation is maintained in the description of the

^{11}Be structure. The resulting calculation is displayed by the dashed line in Fig. 6. Compared to the full XCDCC calculation, this calculation gives fairly less breakup. This effect is similar to that found at $63.7A$ MeV [18], but seems less significant in magnitude at the present lower energy. There is still some small discrepancy of the presented full XCDCC calculations with the amplitude of experimental breakup and elastic scattering cross sections (at the smaller c.m. angles), while the latter one is not observed in the calculations using phenomenological OMPs (see Sec. IV). This might be because of the uncertainties in the fragment-target potentials, the limitations of the structure model used for the ^{11}Be nucleus, or some limitations of the XCDCC method itself.

VI. SUMMARY

The elastic scattering and breakup of ^{11}Be on protons were measured at the incident energy of $26.9A$ MeV. Based on the present and the previous experimental results, a systematic analysis starting from the global optical potentials was carried out and the normalization parameters for the real and imaginary central potentials were obtained. The reduction of the depth of the real central potential and the enhancement of the imaginary part, in comparison to the normal global potentials, are consistent with the effects observed for other weakly bound exotic nuclei.

Calculations with the XCDCC method, which include core excitation effects in ^{11}Be, have been performed and compared with the experimental cross sections. In the case of the elastic scattering, the dynamic core excitation mechanism produces a sizable reduction of the elastic cross sections, which agrees better with the experimental results. For the breakup cross sections corresponding to an excitation energy range of 0.5–3.0 MeV, the full XCDCC calculation gives a better agreement with the experimental data, whereas the calculation without dynamic core excitation results in an overall underestimation. The present analysis confirms the importance of the dynamic core excitation effect for halo nucleus ^{11}Be, which leads to a moderate enhancement of the breakup cross sections and a reduction of the elastic scattering cross sections. This effect was also observed previously to be even stronger at a higher incident energy ($63.7A$ MeV), indicating the necessity of the corresponding treatment in reaction models. The present state-of-the-art XCDCC calculations show a visible improvement in describing the scattering induced by halo nucleus ^{11}Be, although some room for further development still remains, considering the observed discrepancies at small c.m. angles.

[1] A. Ozawa, T. Kobayashi, T. Suzuki, K. Yoshida, and I. Tanihata, Phys. Rev. Lett. **84**, 5493 (2000).

[2] P. G. Hansen and B. Jonson, EPL (Europhys. Lett.) **4**, 409 (1987).

[3] Y. L. Ye, D. Y. Pang, D. X. Jiang, T. Zheng, Q. J. Wang, Z. H. Li, X. Q. Li, Y. C. Ge, C. Wu, G. L. Zhang, Q. Y. Hu, J. Wang, Z. Q. Chen, A. Ozawa, Y. Yamaguchi, R. Kanungo, and I. Tanihata, Phys. Rev. C **71**, 014604 (2005).

[4] J. L. Lou, Y. L. Ye, D. Y. Pang, Z. X. Cao, D. X. Jiang, T. Zheng, H. Hua, Z. H. Li, X. Q. Li, Y. C. Ge, L. H. Lv, J. Xiao, Q. T. Li, R. Qiao, H. B. You, R. J. Chen, H. Sakurai, H. Otsu, M. Nishimura, S. Sakaguchi, H. Baba, Y. Togano, K. Yoneda, C. Li, S. Wang, H. Wang, K. A. Li, T. Nakamura, Y. Nakayama, Y. Kondo, S. Deguchi, Y. Satou, and K. Tshoo, Phys. Rev. C **83**, 034612 (2011).

[5] I. Tanihata, H. Hamagaki, O. Hashimoto, Y. Shida, N. Yoshikawa, K. Sugimoto, O. Yamakawa, T. Kobayashi, and N. Takahashi, Phys. Rev. Lett. **55**, 2676 (1985).

[6] J. S. Al-Khalili and J. A. Tostevin, Phys. Rev. Lett. **76**, 3903 (1996).

[7] K. T. Schmitt, K. L. Jones, A. Bey, S. H. Ahn, D. W. Bardayan, J. C. Blackmon, S. M. Brown, K. Y. Chae, K. A. Chipps, J. A. Cizewski, K. I. Hahn, J. J. Kolata, R. L. Kozub, J. F. Liang, C. Matei, M. Matoš, D. Matyas, B. Moazen, C. Nesaraja, F. M. Nunes, P. D. O'Malley, S. D. Pain, W. A. Peters, S. T. Pittman, A. Roberts, D. Shapira, J. F. Shriner, M. S. Smith, I. Spassova, D. W. Stracener, A. N. Villano, and G. L. Wilson, Phys. Rev. Lett. **108**, 192701 (2012).

[8] R. Palit, P. Adrich, T. Aumann, K. Boretzky, B. V. Carlson, D. Cortina, U. Datta Pramanik, T. W. Elze, H. Emling, H. Geissel, M. Hellström, K. L. Jones, J. V. Kratz, R. Kulessa, Y. Leifels, A. Leistenschneider, G. Münzenberg, C. Nociforo, P. Reiter, H. Simon, K. Sümmerer, and W. Walus, Phys. Rev. C **68**, 034318 (2003).

[9] T. Aumann, A. Navin, D. P. Balamuth, D. Bazin, B. Blank, B. A. Brown, J. E. Bush, J. A. Caggiano, B. Davids, T. Glasmacher, V. Guimarães, P. G. Hansen, R. W. Ibbotson, D. Karnes, J. J. Kolata, V. Maddalena, B. Pritychenko, H. Scheit, B. M. Sherrill, and J. A. Tostevin, Phys. Rev. Lett. **84**, 35 (2000).

[10] J. Winfield, S. Fortier, W. Catford, S. Pita, N. Orr, J. V. de Wiele, Y. Blumenfeld, R. Chapman, S. Chappell, N. Clarke, N. Curtis, M. Freer, S. Gals, H. Langevin-Joliot, H. Laurent, I. Lhenry, J. Maison, P. Roussel-Chomaz, M. Shawcross, K. Spohr, T. Suomijrvi, and A. de Vismes, Nucl. Phys. A **683**, 48 (2001).

[11] N. Fukuda, T. Nakamura, N. Aoi, N. Imai, M. Ishihara, T. Kobayashi, H. Iwasaki, T. Kubo, A. Mengoni, M. Notani, H. Otsu, H. Sakurai, S. Shimoura, T. Teranishi, Y. X. Watanabe, and K. Yoneda, Phys. Rev. C **70**, 054606 (2004).

[12] C. Forssén, P. Navrátil, W. E. Ormand, and E. Caurier, Phys. Rev. C **71**, 044312 (2005).

[13] N. Austern, Y. Iseri, and M. Kamimura, Phys. Rep **154**, 125 (1987).

[14] J. Chen, J. L. Lou, D. Y. Pang, and Y. L. Ye, Sci. China-Phys. Mech. Astron **59**, 632003 (2016).

[15] N. C. Summers, F. M. Nunes, and I. J. Thompson, Phys. Rev. C **74**, 014606 (2006).

[16] A. M. Moro and R. Crespo, Phys. Rev. C **85**, 054613 (2012).

[17] R. Crespo, A. Deltuva, and A. M. Moro, Phys. Rev. C **83**, 044622 (2011).

[18] R. de Diego, J. M. Arias, J. A. Lay, and A. M. Moro, Phys. Rev. C **89**, 064609 (2014).

[19] M. Cortina-Gil, P. Roussel-Chomaz, N. Alamanos, J. Barrette, W. Mittig, F. Dietrich, F. Auger, Y. Blumenfeld, J. Casandjian, M. Chartier, V. Fekou-Youmbi, B. Fernandez, N. Frascaria, A. Gillibert, H. Laurent, A. Lpine-Szily, N. Orr, J. Scarpaci, J. Sida, and T. Suomijrvi, Phys. Lett. B **401**, 9 (1997).

[20] V. Lapoux, N. Alamanos, F. Auger, Y. Blumenfeld, J.-M. Casandjian, M. Chartier, M. Cortina-Gil, V. Fkou-Youmbi, A. Gillibert, M. M. Cormick, F. Marchal, F. Marie, W. Mittig, F. de Oliveira Santos, N. Orr, A. Ostrowski, S. Ottini-Hustache, P. Roussel-Chomaz, J.-A. Scarpaci, J.-L. Sida, T. Suomijrvi, and J. Winfield, Phys. Lett. B **658**, 198 (2008).

[21] N. A. Shrivastava and Y. Blumenfeld, Phys. Lett. B **596**, 54 (2004).

[22] R. L. Varner, Phys. Rep. **201**, 57 (1991).

[23] A. J. Koning and J. P. Delaroche, Nucl. Phys. A **713**, 231 (2003).

[24] T. Shimoda, H. Miyatake, and S. Morinobu, Nucl. Instrum. Methods Phys. Res. Sect. B **70**, 320 (1992).

[25] Z. Cao, Y. Ye, J. Xiao, L. Lv, D. Jiang, T. Zheng, H. Hua, Z. Li, X. Li, Y. Ge, J. Lou, R. Qiao, Q. Li, H. You, R. Chen, D. Pang, H. Sakurai, H. Otsu, M. Nishimura, S. Sakaguchi, H. Baba, Y. Togano, K. Yoneda, C. Li, S. Wang, H. Wang, K. Li, T. Nakamura, Y. Nakayama, Y. Kondo, S. Deguchi, Y. Satou, and K. Tshoo, Phys. Lett. B **707**, 46 (2012).

[26] T. W. Burrows, Phys. Rev. C **7**, 1306 (1973).

[27] T. C. Montgomery, B. E. Bonner, F. P. Brady, W. B. Broste, and M. W. McNaughton, Phys. Rev. C **16**, 499 (1977).

[28] S. Agostinelli, J. Allison, and K. Amako, Nucl. Instrum. Methods Phys. Res. A **506**, 250 (2003).

[29] V. Lapoux and N. Alamanos, Eur. Phys. J. A **51**, 91 (2015).

[30] A. Korsheninnikov, K. Yoshida, D. Aleksandrov, N. Aoi, Y. Doki, N. Inabe, M. Fujimaki, T. Kobayashi, H. Kumagai, C.-B. Moon, E. Nikolskii, M. Obuti, A. Ogloblin, A. Ozawa, S. Shimoura, T. Suzuki, I. Tanihata, Y. Watanabe, and M. Yanokura, Phys. Lett. B **316**, 38 (1993).

[31] C.-B. Moon, M. Fujimaki, S. Hirenzaki, N. Inabe, K. Katori, J. Kim, Y. Kim, T. Kobayashi, T. Kubo, H. Kumagai, S. Shimoura, T. Suzuki, and I. Tanihata, Phys. Lett. B **297**, 39 (1992).

[32] I. J. Thompson, Comput. Phys. Rep. **7**, 167 (1988).

[33] F. Jamil-Qureshi, L. Jian-Ling, and Y. Yan-Lin, Chin. Phys. Lett. **27**, 092501 (2010).

[34] M. E. Brancan and G. R. Satchler, Phys. Rep. **285**, 143 (1997).

[35] K. Yabana, Y. Ogawa, and Y. Suzuki, Nucl. Phys. A **539**, 295 (1992).

[36] F. M. Nunes, J. A. Christley, I. J. Thompson, R. C. Johnson, and V. D. Efros, Nucl. Phys. A **609**, 43 (1996).

[37] S. Karataglidis, K. Amos, and B. G. Giraud, Phys. Rev. C **71**, 064601 (2005).

[38] J. A. Lay, A. M. Moro, J. M. Arias, and J. Gómez-Camacho, Phys. Rev. C **85**, 054618 (2012).

[39] R. A. Malfliet and J. A. Tjon, Nucl. Phys. A **127**, 161 (1969).

[40] M. Takashina and Y. Kanada-Enyo, Phys. Rev. C **77**, 014604 (2008).